

Lu, T.-Y., He, Z.-Y., and Klemm, R., 2021, Identifying crystal accumulation and melt extraction during formation of high-silica granite: *Geology*, <https://doi.org/10.1130/G49434.1>

SUPPLEMENTAL MATERIAL

Identifying crystal accumulation and melt extraction during formation of high-silica granite

Tian-Yu Lu, Zhen-Yu He, and Reiner Klemm

ANALYTICAL METHODS

Zircon U–Pb dating

One granodiorite sample (G427-1), two monzogranite samples (G437-1 and G514-7), one MME sample (G514-3), three rapakivi granite samples (G431-3, G434-1 and G435-1), and two miarolitic granite samples (G429-3 and G431-4) were selected for LA-ICP-MS zircon U–Pb dating. The results are given in Table S1.

Zircon grains were extracted using standard density and magnetic separation techniques. Cathodoluminescence (CL) images of analyzed zircon grains were obtained using an FEI NOVA NanoSEM 450 scanning electron microscope equipped with a Gatan Mono CL4 cathodoluminescence system at the Institute of Geology, Chinese Academy of Geological Sciences. Analytical sites were rechecked under transmitted light images in order to ensure that they were free of visible inclusions and fractures.

In situ zircon U–Pb dating analyses of monzogranite (G437-1), rapakivi granite (G431-3, G434-1 and G435-1), and miarolitic granite (G429-3 and G431-4) samples were carried out using an Agilent 7500a inductively coupled plasma-mass spectrometer (ICP-MS) equipped with a Coherent GeoLas Pro 193-nm laser ablation system at the State Key Laboratory of Mineral Deposits Research, Nanjing University. Analyses were carried out with a beam diameter of 32 μm and 5 Hz repetition rate. Zircon standard GJ-1 was used as external standard to calibrate isotope fractionation (Jackson et al., 2004). Zircon Mud Tank (Black and Gulson, 1978) was frequently analyzed as an independent control on reproducibility and instrument stability. Raw data were processed using GLITTER, which calculated the relevant isotopic ratios, ages and errors, and trace element concentrations (Van Achenbergh et al., 2001). More detailed analytical procedures are described by He et al. (2010).

In situ zircon U–Pb dating of granodiorite (G427-1), monzogranite (G514-7) and MME (G514-3) samples was carried out at the Wuhan Sample Solution Analytical Technology Co., Ltd., using an Agilent 7700e ICP-MS equipped with a Coherent GeoLas Pro 193-nm laser ablation system. The laser frequency was 5 Hz, and the laser-ablation spot diameter was 32 μm . Zircon 91500 (Wiedenbeck et al., 1995) was used as an external standard for calibration of U–Pb isotopic ratios. Zircon standard GJ-1 (Jackson et al., 2004) was used to monitor the stability and accuracy of acquired U–Pb data. Off-line selection and integration of background and analyzed signals, time-drift correction, and quantitative calibration for U–Pb dating were performed by ICPMSDataCal. The detailed analytical procedure and conditions are the same as described by Zong et al. (2017). The weighted mean ages were calculated using IsoplotR (Vermeesch, 2018).

Zircon Hf isotope

Zircon grains from six representative samples were chosen for zircon Hf isotope analysis, including one granodiorite sample (G427-1), one monzogranite sample (G437-1), two rapakivi granite samples (G431-3 and G435-1), and two miarolitic granite samples (G429-3 and G431-4). The zircon Hf isotopic compositions are listed in Table S2.

Zircon Hf isotope analyses of monzogranite (G437-1), rapakivi granite (G431-3 and G435-1), and miarolitic granite (G429-3 and G431-4) were carried out *in situ* using a Neptune Plus multi-collector inductively coupled plasma mass spectrometer (MC-ICP-MS) in combination with a GeoLas 2005 excimer ArF laser ablation system at the State Key Laboratory of Geological Processes and Mineral Resources, China University of Geosciences (Wuhan). The energy density of the laser ablation was 5.3 J/cm² and the ablation spot was 44 μm in diameter. In order to evaluate the reliability of the analytical data, standard zircon 91500 and TEMORA were analyzed during the course of this study and yielded mean ¹⁷⁶Hf/¹⁷⁷Hf values of 0.282308 ± 13 (2 σ ; n = 20) and 0.282701 ± 32 (2 σ ; n = 4). Detailed operating conditions for the laser ablation system and the MC-ICP-MS instrument and analytical method are similar to those described by Hu et al. (2012).

Zircon Hf isotope analyses of granodiorite (G427-1) were carried out *in situ* using a Neptune Plus MC-ICP-MS in combination with a Coherent GeoLas Pro 193-nm laser ablation system at the Wuhan Sample Solution Analytical Technology Co., Ltd. The spot size is 44 μm . The energy density of laser ablation that was used in

this study was $\sim 7.0 \text{ J/cm}^2$. Each measurement consisted of 20 s of acquisition of the background signal followed by 50 s of ablation signal acquisition. Analyses of zircon standards 91500 and TEMORA were used as external standards to evaluate the reliability of the analytical data, yielded mean $^{176}\text{Hf}/^{177}\text{Hf}$ values of 0.282309 ± 10 (2σ ; $n = 3$) and 0.282675 ± 28 (2σ ; $n = 4$), respectively. Detailed operating conditions for the laser ablation system and the MC-ICP-MS instrument and analytical method are similar to those described by [Hu et al. \(2012\)](#).

The measured $^{176}\text{Lu}/^{177}\text{Hf}$ ratios and the ^{176}Lu decay constant of $1.867 \times 10^{-11} \text{ yr}^{-1}$ ([Söderlund et al., 2004](#)) were used to calculate the initial $^{176}\text{Hf}/^{177}\text{Hf}$ ratios. The chondritic values of [Bouvier et al. \(2008\)](#) were used to calculate the $\epsilon_{\text{Hf}}(t)$ values. The depleted mantle Hf model age (T_{DM}) was calculated using the analyzed $^{176}\text{Lu}/^{177}\text{Hf}$ value of zircon and depleted mantle values of [Griffin et al. \(2000\)](#). The crustal model age (T_{DMC}) was calculated using a $^{176}\text{Lu}/^{177}\text{Hf}$ ratio of 0.015 for an average continental crust ([Griffin et al., 2002](#)).

Whole-rock major and trace element

Whole-rock geochemical data for different units of the Nyemo composite pluton are listed in Table S3.

Whole-rock major element analysis was performed using a Rigaku3080 X-ray fluorescence spectrometer (XRF) at the National Research Center for Geoanalysis, Chinese Academy of Geological Sciences. The analytical precision was generally better than 2% for all elements. Trace element abundances were measured by Wuhan Sample Solution Analytical Technology Co., Ltd., using an Agilent 7700e ICP-MS, which gives a precision better than 10% for most of the analyzed elements. For detailed sample-digesting and analytical procedures, see [Zong et al. \(2017\)](#). In Fig. 3A and B, chondrite values are from [Sun and McDonough \(1989\)](#) and primitive mantle values from [McDonough et al. \(1992\)](#).

Zircon trace element

Zircons trace element compositions from different units of the Nyemo composite pluton are listed in Table S4.

In situ zircon trace element analyses were obtained at the GeoZentrum Nordbayern, Friedrich-Alexander Universität Erlangen-Nürnberg, Germany, using a single collector quadrupole Agilent 7500c ICP-MS equipped with a 193 nm Analyte Excite laser ablation system (Teledyne Photon Machines). The measurements were conducted using a laser frequency of 20 Hz and ^{29}Si concentrations were used as

internal standard. According to the respective zircon grain size, a spot diameter of 25 μm was chosen but smaller domains were analyzed using a spot diameter of 20 μm . The acquisition time for each analysis was 45 s including 20 s for background scanning. Repeated measurements on the glass reference material NIST SRM 612 (Pearce et al., 1997) were used for external calibration. The international reference material BCR-2G and zircon 91500 was used to check the reproducibility and accuracy (Jacob, 2006). Detailed analytical procedures and data reduction procedures are described in Yan et al. (2020).

MODELING SETUP FOR MAGMATIC EVOLUTION

Assimilation-fractional and/or fractional crystallization

During the fractional crystallization (FC; Rayleigh fractionation, Rayleigh, 1896) process, early formed phases are continuously removed from the liquid during crystallization of the magma. It is expressed by the equations $C_l^{FC} = C_0 F^{(D-1)}$ and $C_r^{FC} = C_0 \frac{1-F^D}{1-F}$ where C_l^{FC} is the trace element concentration in the remaining melt, C_r^{FC} is the trace element concentration in the total residual solid, C_0 is the concentration of the trace element in parental magma (starting composition), D is the bulk partition coefficient of the elements for fractionating mineral phases, F is the fraction of melt remaining during crystallization. During the assimilation-fractional crystallization (AFC) process there is a strict relationship between the amount of material assimilated and the amount of material crystallized during cooling of the magma. Thus, it is expressed by the equation $C_l^{AFC} = C_0 [F^{-z} + \left(\frac{r}{r-1}\right) \frac{C_a}{zC_0} (1 - F^{-z})]$ where C_l^{AFC} , C_0 , and C_a are the trace element concentrations in the resulting magma, parental magma, and assimilating material (wall rock), respectively. F is the fraction of melt during cooling of the magma and r is the ratio of the assimilation rate to the fractional crystallization rate. The z value in AFC equation is expressed by the equation $z = \frac{r+D-1}{r-1}$ where D is the bulk partition coefficient of the elements for fractionating mineral phases. In the case of $r = 0$, the equation represents pure fractional crystallization. Equations are from Albarede (1995).

Model setup for the mafic magma evolution curves in Fig. 2C use the gabbro sample (Rb = 16.6 ppm and Sr = 836 ppm; NM1711) as starting composition. Samples with higher Sr and lower Rb could be partly cumulative. We selected a schist

from the Sangri volcanic succession in the Nyemo area (Rb = 29.7 ppm and Sr = 305 ppm; sample 2-1 from [Dong et al., 2018](#)) as the assimilating material. Tick marks indicate the fraction percent of melt remaining during crystallization. Fractionating mineral assemblage and partition coefficient values are given in Table S5. The silicic evolution models in Fig. 3C and D use the granodiorite sample (15TNM06) as the starting composition. Melt evolution determined by the Rayleigh fractionation and bulk cumulation. Plots use a range of published end-member solid-melt partition coefficients to create bracketing models (bulk $D_{Rb} = 0.51-1.58$, bulk $D_{Eu} = 2.08-5.69$ and bulk $D_{Ba} = 2.70-12.0$). Tick marks indicate the fraction percent of melt remaining. Fractionating mineral assemblage and partition coefficient values are given in Table S6. In addition, a zircon sample (G427-1-05) from the granodiorite is chosen as the starting composition for evolution models in Fig. 4B and C. They show the same evolution processes and fractionating mineral assemblage as those in Fig. 3C and D. More calculation details and partition coefficient values are given in Table S7.

Crystal-melt partitioning model

Partition coefficients for many elements incorporated in zircon are highly dependent on the structural strain associated with coupled substitutions (e.g., [Hanchar and van Westrenen, 2007](#)) and are modestly to strongly temperature-dependent (e.g., [Rubatto and Hermann, 2007](#)). Based on the observation that the mineral/melt partition coefficients for isovalent cations show a near-parabolic dependence on the cation radius ([Onuma et al., 1968](#)), [Blundy and Wood \(1994\)](#) used the lattice strain model of [Brice \(1975\)](#) to define the equation: $D_i = D_0 \times \exp \left\{ \frac{-4\pi EN_A \left[\frac{r_0}{2}(r_i - r_0)^2 + \frac{1}{3}(r_i - r_0)^3 \right]}{RT} \right\}$ where D_i is the trace element partition coefficient, r_i is the trace element ionic radius, r_0 is the ideal radius (in Å), D_0 is the theoretical partition coefficient for an element with ideal radius, E is Young's modulus (in GPa), N_A is Avogadro's number, R is the gas constant, T is the temperature (in K). As expected for a consistent partitioning model (e.g., [Green et al., 2000](#)), [Rubatto and Hermann \(2007\)](#) firstly reported that the theoretical partition coefficient D_0 systematically decreases with increasing T for zircon/melt partitioning and gave a linear regression of $\ln D_0$ versus $1/T$ (in K): $\ln D_0 = -14.221 + 22420/T$.

The lattice strain model setup in Fig. 4D uses the same Young's modulus E and ideal radius r_0 . The Young's modulus E (450 GPa) is constant over the T series, and the ideal radius r_0 (0.90 Å) is close to the ionic radius of Zr for which the REE

substitute, both of which are similar to those of [Rubatto and Hermann \(2007\)](#). The Avogadro's number N_A is $6.022 \times 10^{23} \text{ mol}^{-1}$ and the gas constant R is $8.314 \text{ J} \cdot \text{K}^{-1} \cdot \text{mol}^{-1}$ ([Mills et al., 1993](#)). The lattice strain least-squares fits to the curves are only approximated. More details and the ionic radius ([Shannon, 1976](#)) for REE are given in Table S8.

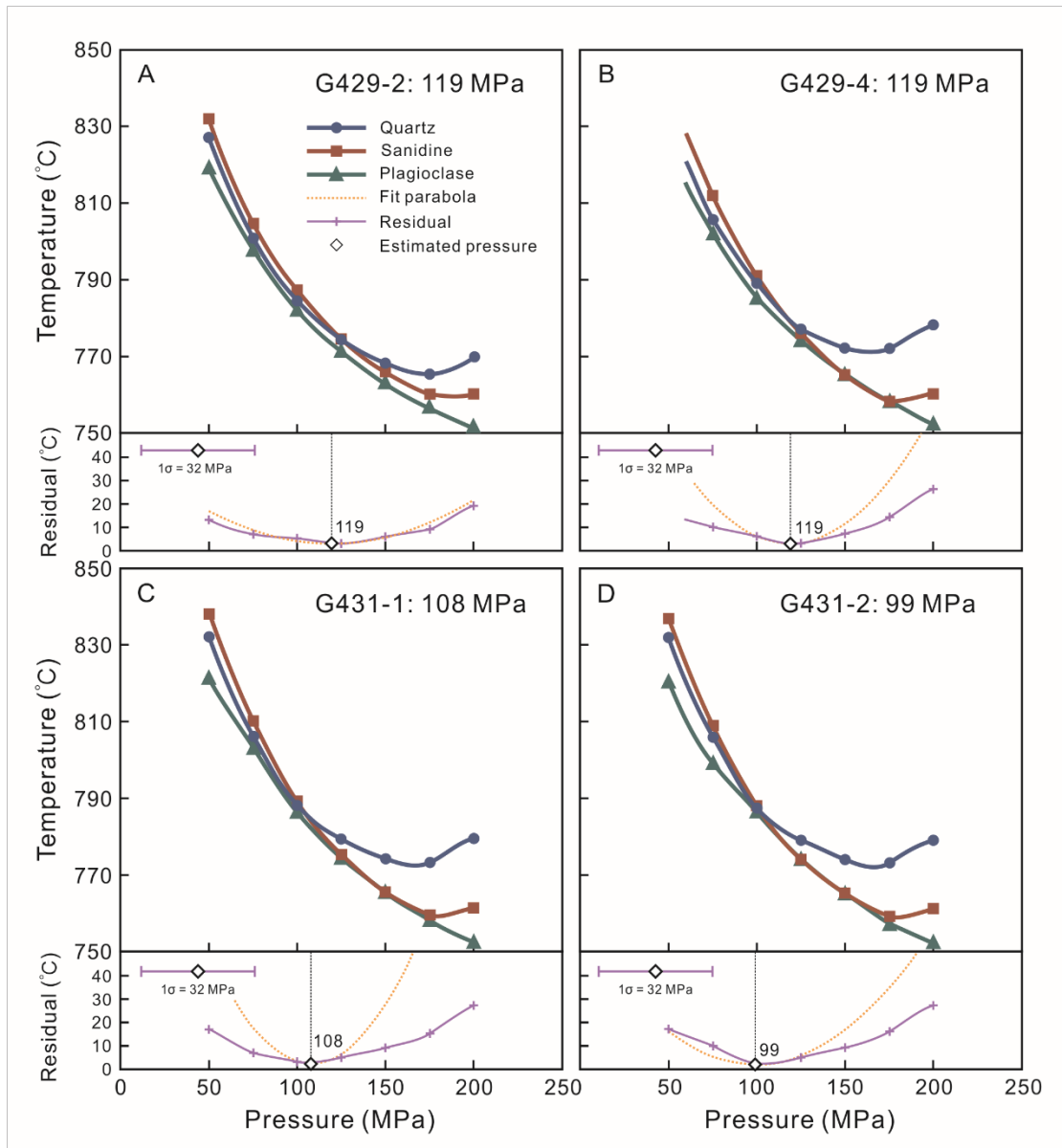


Figure S1. Application of the rhyolite-MELTS geobarometer ([Gualda and Ghiorso, 2014](#)) to miarolitic granite from the Nyemo composite pluton. The estimated pressure corresponds to the minimum of the fit parabola calculated for the residual temperature curve (difference between the quartz and plagioclase saturation curves). Error bars represent uncertainty in pressure estimations, following the approach given by [Gualda and Ghiorso \(2014\)](#) and [Pitcher et al. \(2021\)](#).

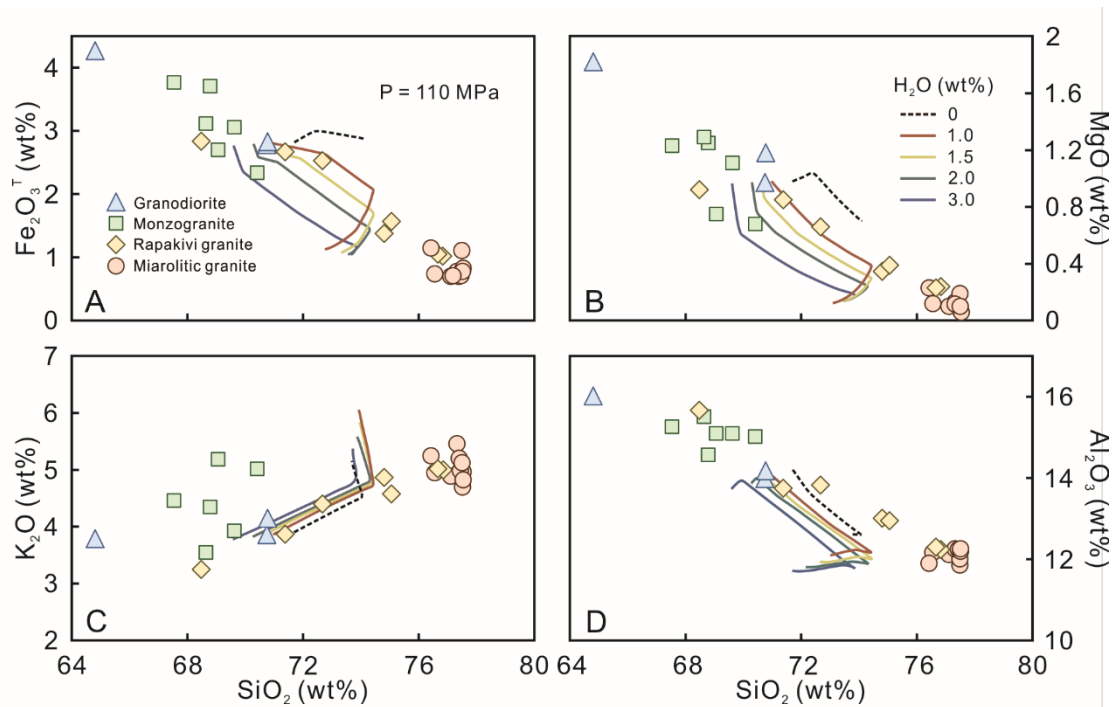


Figure S2. Harker diagrams for different units of the Nyemo composite pluton, exhibiting well-defined chemical variation trends. Curves in the diagrams represent rhyolite-MELTS (Gualda et al., 2012) thermodynamic models by crystallization of the silicic parent for an estimated pressure of ~ 110 MPa and different bulk H_2O contents ($f\text{O}_2$ at the fayalite-magnetite-quartz buffer).

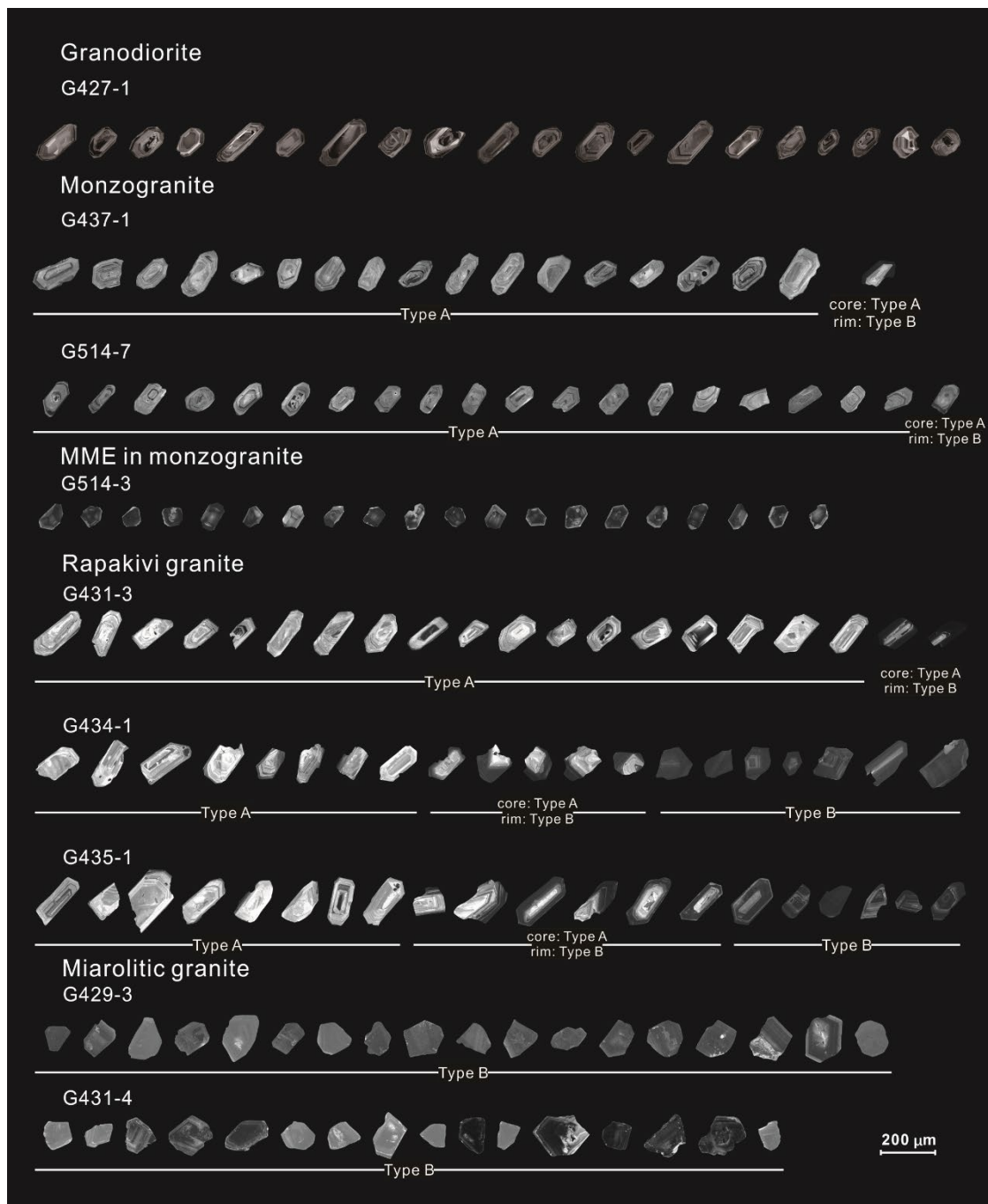


Figure S3. CL images of representative zircon grains from different units of the Nyemo composite pluton. Note: Type B zircons from samples G437-1, G514-7 and G431-3 were not analyzed due to their small size.

REFERENCES CITED

- Albarede, F., 1995, *Introduction to geochemical modeling*: New York, Cambridge University Press, 543 p.
- Black, L.P., and Gulson, B.L., 1978, The age of the Mud Tank carbonatite, Strangways Range, Northern Territory: *BMR Journal of Australian Geology and Geophysics*, v. 3, p. 227–232.
- Blundy, J.D., and Wood, B.J., 1994, Prediction of crystal–melt coefficients from elastic moduli: *Nature*, v. 372, p. 452–454.
- Bouvier, A., Vervoort, J.D., and Patchett, P.J., 2008, The Lu-Hf and Sm–Nd isotopic composition of CHUR: Constraints from unequilibrated chondrites and implications for the bulk composition of terrestrial planets: *Earth and Planetary Science Letters*, v. 273, p. 48–57.
- Brice, J.C., 1975, Some thermodynamic aspects of the growth of strained crystals: *Journal of Crystal Growth*, v. 28, p. 249–253.
- Dong, X., Zhang, Z., Klemd, R., He, Z., and Tian, Z., 2018, Late Cretaceous tectonothermal evolution of the southern Lhasa terrane, South Tibet: Consequence of a Mesozoic Andean-type orogeny: *Tectonophysics*, v. 730, p. 100–113.
- Griffin, W.L., Pearson, N.J., Belousova, E., Jackson, S.E., van Achterbergh, E., O'Reilly, S.Y., and Shee, S.R., 2000, The Hf isotope composition of cratonic mantle: LAM-MC-ICPMS analysis of zircon megacrysts in kimberlites: *Geochimica et Cosmochimica Acta*, v. 64, p. 133–147.
- Griffin, W.L., Wang, X., Jackson, S.E., Pearson, N.J., O'Reilly, S.Y., Xu, X., and Zhou, X., 2002, Zircon chemistry and magma mixing, SE China: In situ analysis of Hf isotopes, Tonglu and Pingtan igneous complexes: *Lithos*, v. 61, p. 237–269.
- Green, T.H., Blundy, J.D., Adam, J., and Yaxley, G.M., 2000, SIMS determination of trace element partition coefficients between garnet, clinopyroxene and hydrous basaltic liquids at 2–7.5 GPa and 1080–1200 °C: *Lithos*, v. 53, p. 165–187.
- Gualda, G.A.R., and Ghiorso, M.S., 2014, Phase-equilibrium geobarometers for silicic rocks based on rhyolite-MELTS. Part 1: Principles, procedures, and evaluation of the method: *Contributions to Mineralogy and Petrology*, v. 168, 1033.
- Gualda, G.A.R., Ghiorso, M.S., Lemons, R.V., and Carley, T.L., 2012, Rhyolite-MELTS: A modified calibration of MELTS optimized for silica-rich, fluid-bearing magmatic systems: *Journal of Petrology*, v. 53, p. 875–890.
- Hanchar, J.M., and van Westrenen, W., 2007, Rare earth element behavior in zircon-melt systems: *Elements*, v. 3, p. 37–42.
- He, Z., Xu, X., Zou, H., Wang, X., and Yu, Y., 2010, Geochronology, petrogenesis and metallogeny of Piaotang granites in the tungsten deposit region of South China: *Geochemical Journal*, v. 44, p. 299–313.
- Hu, Z., et al., 2012, Improved in situ Hf isotope ratio analysis of zircon using newly designed X skimmer cone and Jet sample cone in combination with the addition

- of nitrogen by laser ablation multiple collector ICP-MS: *Journal of Analytical Atomic Spectrometry*, v. 27, p. 1391–1399.
- Jacob, D.E., 2006, High sensitivity analysis of trace element-poor geological reference glasses by laser ablation–inductively coupled plasma–mass spectrometry (LA-ICP-MS): *Geostandards and Geoanalytical Research*, v. 30, p. 221–235.
- Jackson, S.E., Pearson, N.J., Griffin, W.L., and Belousova, E.A., 2004, The application of laser ablation–inductively coupled plasma–mass spectrometry to in situ U-Pb zircon geochronology: *Chemical Geology*, v. 211, p. 47–69.
- McDonough, W.F., Sun, S.-S., Ringwood, A.E., and Hofmann, A.W., 1992, Potassium, rubidium, and cesium in the Earth and Moon and the evolution of the mantle of the Earth: *Geochimica et Cosmochimica Acta*, v. 56, p. 1001–1012.
- Mills, I., Cvitaš, T., Homann, K., Kallay, N., and Kuchitsu, K., 1993, *Quantities, Units and Symbols in Physical Chemistry (second edition)*: Oxford, International Union of Pure and Applied Chemistry, Blackwell Science.
- Onuma, N., Higuchi, H., Wakita, H., and Nagasawa, H., 1968, Trace element partition between two pyroxenes and the host lava: *Earth and Planetary Science Letters*, v. 5, p. 47–51.
- Pearce, N.J.G., Perkins, W.T., Westgate, J.A., Gorton, M.P., Jackson, S.E., Neal, C.R., and Chenery, S.P., 1997, A compilation of new and published major and trace element data for NIST SRM 610 and NIST SRM 612 glass reference materials: *Geostandards and Geoanalytical Research*, v. 21, p. 115–144.
- Pitcher, B.W., Gualda, G.A.R., and Hasegawa, T., 2021, Repetitive duality of rhyolite compositions, timescales, and storage and extraction conditions for Pleistocene caldera-forming eruptions, Hokkaido, Japan: *Journal of Petrology*, v. 62, ega106.
- Rayleigh, J.W.S., 1896, Theoretical considerations respecting the separation of gases by diffusion and similar processes: *Philosophical Magazine*, v. 42, p. 77–107.
- Rubatto, D., and Hermann, J., 2007, Experimental zircon/melt and zircon/ garnet trace element partitioning and implications for the geochronology of crustal rocks: *Chemical Geology*, v. 241, p. 38–61.
- Shannon, R.D., 1976, Revised effective ionic radii and systematic studies of interatomic distances in halides and chalcogenides: *Acta crystallographica section A: crystal physics, diffraction, theoretical and general crystallography*, v. 32, p. 751–767.
- Söderlund, U., Patchett, P.J., Vervoort, J.D., and Isachsen, C.E., 2004, The ^{176}Lu decay constant determined by Lu-Hf and U-Pb isotope systematics of Precambrian mafic intrusions: *Earth and Planetary Science Letters*, v. 219, p. 311–324.
- Sun, S.-S., and McDonough, W.F., 1989, Chemical and isotopic systematics of oceanic basalts: Implications for mantle composition and processes: *Geological Society, London, Special Publication*, v. 42, p. 313–345.
- Van Achterbergh, E., Ryan, C.G., Jackson, S.E., and Griffin, W.L., 2001, Data reduction software for LA-ICP-MS: Appendix, in Sylvester, P.J., ed., *Laser Ablation-ICP-Mass Spectrometry in the Earth Sciences: Principles and*

- Applications. Mineralogical Association of Canada Short Course Series, v. 29, p. 39–243.
- Vermeesch, P., 2018, IsoplotR: A free and open toolbox for geochronology: *Geoscience Frontiers*, v. 9, p. 1479–1493.
- Wiedenbeck, M., Allé, P., Corfu, F., Griffin, W.L., Meier, M., Oberli, F., Von Quadt, A., Roddick, J.C., and Spiegel, W., 1995, Three natural zircon standards for U–Th–Pb, Lu–Hf, trace element and REE analyses: *Geostandards and Geoanalytical Research*, v. 19, p. 1–23.
- Yan, L.L., He, Z.Y., Klemd, R., Beier, C., and Xu, X.S., 2020, Tracking crystal-melt segregation and magma recharge using zircon trace element data: *Chemical Geology*, v. 542, 119596.
- Zong, K., Klemd, R., Yuan, Y., He, Z., Guo, J., Shi, X., Liu, Y., Hu, Z., and Zhang, Z., 2017, The assembly of Rodinia: The correlation of early Neoproterozoic (ca. 900 Ma) high-grade metamorphism and continental arc formation in the southern Beishan Orogen, southern Central Asian Orogenic Belt (CAOB): *Precambrian Research*, v. 290, p. 32–48.